Truly 3D Midsagittal Plane Extraction for Robust Neuroimage Registration *

Leonid Teverovskiy Yanxi Liu

CMU-RI-TR-04-21

March 2004

Robotics Institute
Carnegie Mellon University
Pittsburgh, Pennsylvania 15213

*This work is partially supported by NIH grant R21 DA015900-01

Abstract

This paper describes a robust algorithm for reliable ideal Midsagittal Plane extraction (iMSP) from 3D neuroimages. The algorithm makes no assumptions about initial orientation of a given 3D brain image and works reliably on neuroimages of normal brains as well as brains with significant pathologies. Presented technique is truly three-dimensional since we treat each neuroimage as a three-dimensional volume rather than a set of two-dimensional slices. We use an edge-based approach which employs cross-correlation to extract iMSP. This work also includes quantitative evaluation of the performance of the proposed algorithm when applied to a wide variety of real neuroimages. We find that our algorithm is able to extract iMSP from neuroimages with arbitrary initial orientations, large asymmetries, and low signal to noise ratio. We also demonstrate how presented algorithm can increase robustness of existing neuroimage registration algorithms, be it rigid, affine or less restricted deformable registration. Our algorithm was implemented using Insight Toolkit(ITK).

Contents

1. Introduction

In many neuroimage processing and classification tasks [12, 10, 11] it is imperative to be able to calculate the exact location of the midsagittal plane. Performing statistical quantification of human brain asymmetry [4, 5, 19], for example, is impossible without knowing where the plane of symmetry is. In many classification problems symmetry based features are informative and increase discriminative power of the feature vector. In the process of registering a pair of neuroimages to each other, knowledge of the midsagittal plane locations makes it possible to find a good initial mutual orientation of the neuroimages. Moreover, if the locations of midsagittal planes are known, the number of parameters that have to be estimated during registration can be reduced. In the case of affine registration, for instance, the number of estimated parameters can be reduced from twelve to eight. Another possible application of the midsagittal plane extraction algorithm is in bringing neuroimages into standard coordinate system, like commonly used Talairach coordinate system [18], automatically. Talairach framework relies on landmarks and defines principal orthogonal coordinate axes based on interhemispheric midsagittal plane, AC-PC line [1] and VAC line[2]. However, in some normal brains and in many pathological brains with tumors or lesions interhemispheric midsagittal plane is not a geometric plane but a curved two-dimensional surface. In such cases, therefore, the coordinate axis based on interhemispheric midsagittal plane in Talairach coordinate system is defined ambiguously. This fundamental ambiguity can be removed by defining an ideal midsagittal plane (iMSP).

Ideal midsagittal plane is a virtual geometric plane about which the three-dimensional anatomical structure captured in the given neuroimage exhibits maximum bilateral symmetry [12]. It is the location of this plane that is useful to know. However, fully automatic extraction of iMSP presents a number of challenges posed by various extrinsic and intrinsic factors. First, successful algorithm should work for a wide variety of initial orientations of a given three dimensional neuroimage without assuming that a set of two-dimensional slices representing it is axial, coronal or sagittal. In the emergency room conditions, where a patient might be unconscious, the two-dimensional slices out of a scanner can be neither coronal nor axial nor sagittal unless pre-scanning alignment is used. Automated MSP extraction algorithm with no limitations on the initial orientation of the unput neuroimage can be used to eliminate the need for such alignment, thus reducing medical imaging costs. Second, performance of the algorithm should not deteriorate when large degree of asymmetry is present in a given neuroimage. Some brains, especially the ones with pathologies, can significantly deviate from being symmetric. This fact may be due to the presence of a stroke or a tumor in the brain. Third, the algorithm should reliably find iMSP even if given neuroimage has low signal to noise ratio. This paper presents a fully automated algorithm for iMSP extraction that satisfies these three criteria. Section 2 reviews existing work on automatic MSP extraction. Section 3 describes proposed algorithm for automatic ideal midsagittal plane extraction. Section 4 contains quantitative evaluation of the algorithm's performance when applied to normal, highly asymmetric and noisy neuroimages. Section 5 illus-

[1] line passing through the superior aspect of the anterior commissure (AC) and the inferior aspect of the posterior commissure (PC)

[2] line passing through the posterior margin of anterior commissure and perpendicular to AC-PC line

trates advantages of using the algorithm as a preprocessing step of registration process, and, finally, in section 6 we present a brief summary of the paper.

2. Related Work

We can divide existing MSP extraction algorithms into 2 conceptually different groups. First group of algorithms defines MSP in terms of anatomical structures of the brain [2]. Such methods assume that the interhemispheric fissure of the brain is approximately planar and is, in fact, a good approximation to MSP. Therefore, they identify task of estimating MSP with the task of detecting the interhemispheric fissure. Once the fissure is found, its location is used to estimate MSP. The fact that interhemispheric fissure is often not planar even in normal brains limits robustness of this kind of approaches. Also, such algorithms are sensitive to modality of the image, image artifacts, and often require segmentation as a preprocessing step.
The other group of techniques defines MSP as a symmetry plane of a neuroimage [1, 6, 7, 12, 15]. Methods in this group usually define a symmetry measure and find a plane which maximizes it. Depending on the type of symmetry measure and whether it is applied to the original intensity image or to a volume that was preprocessed, the algorithms in this group can be affected by the global asymmmetry of the brain. This is because if the brain is significantly tilted, corresponding left and right anatomical structures of the brain do not appear on the same slice. Consequently, symmetry lines which are computed on each 2D slice are meaningless and lead to erroneous estimations of MSP. 3D methods that compute symmetry measure on the entire volume have the potential of overcoming the neuroimage orientation constraint of 3D slice based algorithms. A different approach is employed by Prima, et al [17]. They utilize deformable registration and block matching to compute MSP. However, they report that their approach breaks if the yaw and roll angles of the given neuroimage are about 21 degrees [17]. This is approximately the same as the breaking point reported by Liu et al [12] for their algorithm where midsagittal plane was estimated from a set of 2D slices.

3. Ideal Midsagittal Plane Extraction Algorithm.

In this section we present an algorithm for extracting ideal midsagittal plane from an *arbitrarily* oriented three-dimensional neuroimage represented by a set of two-dimensional slices. In order to describe our algorithm we will first describe preprocessing operations we perform on the input neuroimage, then we specify three general components of our algorithm: our parametrization of the space of possible solutions, the metric to evaluate candidate solutions, and the exploration strategy for this parametrized space.

3.1 Preprocessing

In order to increase robustness of our algorithm, we must reduce its sensitivity to such factors as noise, bias fields and asymmetries of the brain, whether natural or caused by a disease. We achieve this goal by anisotropic smoothing, subsampling and edge

detection [3, 16]. Subsampling makes our algorithm insensitive to minor asymmetries of the brain. Anisotropic smoothing reduces noise in the image while preserving edges. Finally, edge detection reduces effects of the remaining noise and bias field and forces our algorithm to consider only main structures in the brain. In addition, edge detection allows us to use computationally effective measure of symmetry.

3.2 Parametrization of the Space of Possible Solutions

In our problem of extracting ideal midsagittal plane, the space of possible solutions is a set of all possible planes. In order to be able to explore this space we must parametrize it first.

Given a stack of 2-D slices representing a 3-D neuroimage, we define a coordinate system as follows. The origin of the system coincides with the bottom left corner of the first slice; x-axis corresponds to the bottom horizontal edge of the first slice; y-axis corresponds to the left vertical edge of the slice, and z-axis is perpendicular to the first slice and directed toward last slice. We measure distances along each axes in voxels. For example, if voxel has dimensions $[\ x \quad y \quad z\ ] = [\ 0.9375mm \quad 0.9375mm \quad 1.5mm\ ]$ then a point with coordinates $[\ 1 \quad 2 \quad 3\ ]$ in introduced coordinate system will have physical coordinates of $[\ 0.9375mm \quad 0.9375mm \quad 1.5mm\ ]$. We define any plane by a point **P** on the plane and its normal vector $\vec{V}$. The latter can be given by a vector of unit length $\vec{V}$. Thus, we can now traverse the space of possible solutions by changing coordinates of **P** and $\vec{V}$.

3.3 Metric to Evaluate Possible Solutions

Given a particular instantiation of the point **P** and the unit normal vector $\vec{V}$, we need to be able to evaluate how symmetric the input neuroimage is with respect to the plane specified by these **P** and $\vec{V}$, and do it in a computationally efficient way. For our evaluation measure we choose correlation of original neuroimage and its flipped copy about a given plane [14, 15, 9].

$$S = \frac{\sum_i^w \sum_j^h \sum_k^d I^o_{ijk} I^f_{ijk}}{\sqrt{\left(\sum_i^w \sum_j^h \sum_k^d I^f_{ijk} I^f_{ijk}\right)\left(\sum_i^w \sum_j^h \sum_k^d I^o_{ijk} I^o_{ijk}\right)}} \tag{1}$$

where w, h, d are respectively width, height and depth of the 3D neuroimage, I^o_{ijk} is intensity value of the voxel with coordinates i, j, k in the original image, I^f_{ijk} is intensity value of the voxel with coordinates i, j, k in the flipped image.

After preprocessing, we transform the original neuroimage into a binary edge image. (1) reduces to

$$S = \frac{M}{\sqrt{N \cdot N}} = \frac{M}{N} \tag{2}$$

where N is the total number of non-zero voxels in the binary image, M is the total number of coordinate triples for which voxels in both original and flipped binary neuroimages have non-zero values. The formula (2) suggests that we only need to loop

through non-zero voxels of the binary edge image, which makes the evaluation process much faster.
Finally, we avoid actually flipping the 3D neuroimages by using the following formulas to relate coordinates of a voxel to coordinates of the voxel that would have corresponded to it had we flipped the image about a given plane.

$$\overrightarrow{A^f} = \overrightarrow{A^o} + 2\left[\overrightarrow{(H * A^o - A^o)} + \overrightarrow{(P - H * P)}\right] \quad (3)$$

where A^o is the voxel under consideration, A^f the voxel that would have corresponded to A^o had we flipped the image about a given plane, $\vec{A^o}$is a vector starting at the origin and ending in A^o, $\vec{A^f}$ is a vector starting at the origin and ending in A^f, H is a projection matrix which projects onto the plane defined by given **P** and $\vec{V}$.

$$H = [\vec{W}\vec{U}\vec{0}] \times [\vec{W}\vec{U}\vec{V}]^{-1} \quad (4)$$

where $\vec{W}$ and $\vec{U}$ are unit vector which together with $\vec{V}$ form an orthogonal basis.

3.4 Exploration Strategy for the Parametrized Space of Possible Solutions

The parametrization we use indexes the space of candidate midsagittal planes by two continuous parameters: point **P** and unit vector $\vec{V}$. We cannot search this space exhaustively, therefore we traverse the space in the following manner.
Given $\vec{V}$ we will change the coordinates of **P** by $\vec{V}$ at a time. This corresponds to moving a plane by 1 unit at a time in the direction perpendicular to the plane. Moreover, since we are looking for the plane of symmetry, we will require that candidate planes be close to the centroid of the given neuroimage. Thus, given $\vec{V}$, we will only consider a relatively small set of planes located near centroid that are perpendicular to $\vec{V}$.
However, we cannot impose any restrictions on $\vec{V}$ since one of the goals of our algorithm is to extract ideal midsagittal plane from 3D neuroimages with arbitrary orientation. To visualize the search strategy we employ, imagine that the unit vector $\vec{V}$ is at the center of a unit sphere. Then to consider all possible values for $\vec{V}$ means to sweep the entire surface of the sphere with the endpoint of $\vec{V}$. We will embed a lattice into the surface of the sphere and visit only nodes of this lattice. Moreover we can eliminate half of the sphere from the consideration because $\vec{V}$ and -$\vec{V}$ specify the same orientation of the plane perpendicular to them. Thus, each visited node corresponds to a particular orientation of $\vec{V}$. Fixing $\vec{V}$, we now change **P** as described above, and retrieve the plane with the maximum correlation score computed according to (2). In such a way we can assign a score to each of the $\vec{V}'s$. In order to make our algorithm more robust to spurious matches, we will choose a set of $\vec{V}'s$ with highest scores rather than a single $\vec{V}$ with the highest score for further exploration. For each selected $\vec{V}$ we embed a finer lattice around the node which corresponds to it and then visit every

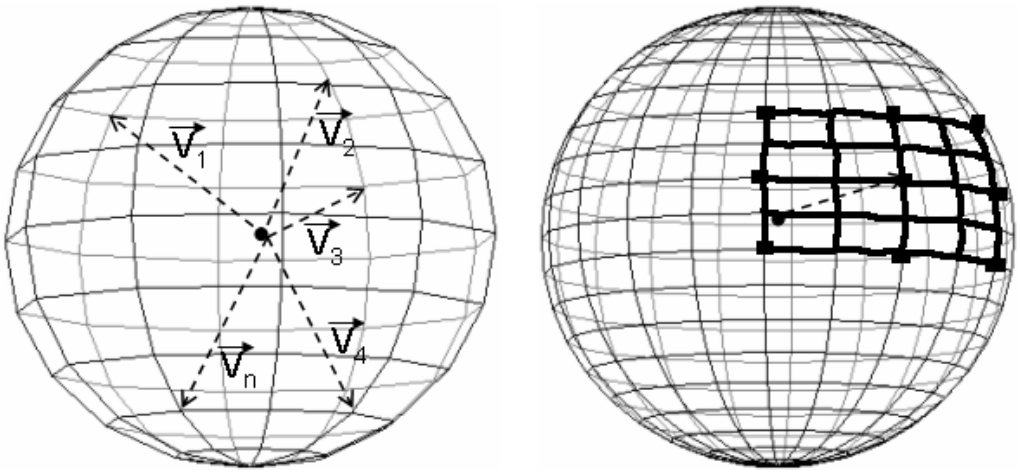

Figure 1: We embed a coarse lattice on the surface of a unit sphere and make the endpoint of $\vec{V}$ visit every node of the lattice. The leftmost sphere depicts this process. Then we embed a finer lattice around each of the five nodes of the coarse lattice that have highest symmetry measure value. The rightmost sphere shows one of these 5 nodes, together with finer lattice embedded in its neighborhood.

node of that finer lattice. For each of the finer lattices we pick a node with the highest score and subsequently choose the node which gives the highest score as evaluated on the full size edge image. After that we embed yet another even finer lattice around the selected node and evaluate the nodes of the lattice according to the formula (2) as applied to full sized edge image. The evaluation of the finest lattice produces $\vec{V}$ and **P** that correspond to the ideal midsagittal plane. Figure 3 provides pseudocode of our algorithm along with step by step illustration of its work.

4. Evaluation

In this section we will quantitatively characterize robustness of the proposed iMSP extraction algorithm. As the measure of error of our algorithm we will use angle α, in degrees, between vector normal to true iMSP, $\vec{V}$, and vector normal to an iMSP estimated by the algorithm, $\hat{\vec{V}}$.

4.1 Data

We will test our algorithm on 19 3D MR neuroimages. Since these images were acquired in controlled environment, their true iMSP is not far from being parallel to yz-plane. For convenience, the images were resampled to have cubic voxels and dimensions of 256x256x256 voxels. We call this dataset *Normal*. Three additional datasets are created based on this *Normal* dataset. In order to investigate how various imaging

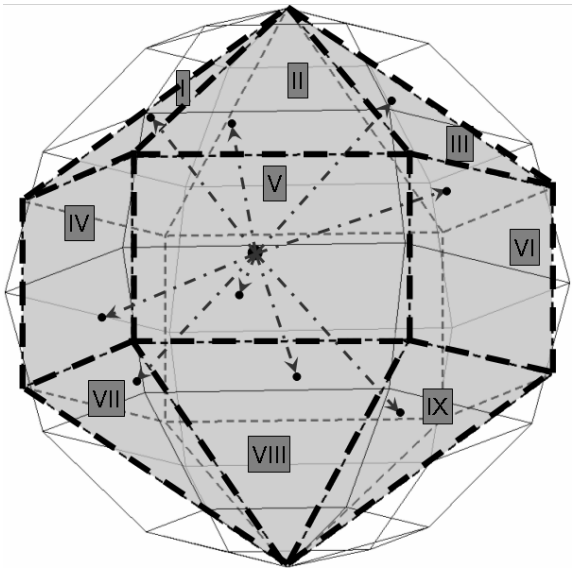

Figure 2: The figure demonstrates the way we partition the unit hemisphere into sectors and introduces the numbering of the sectors

Table 1: Parameters of simulated tumors and noise. First row contains neuroimage number. We group two different neuroimages in the same column if they have the same noise and simulated tumors added. Second row characterizes absolute strength of the artificially added noise and contains signal to noise ratio, in dBW, of the noise if the signal strength were 0 dBW. The remaining rows contain x, y and z coordinates of the center of a simulated tumor and the radius of the tumor, in voxels

Neuroimage #	1, 6	2, 7	3, 8	4, 9	5	10	11	12	13	14	15	16	17	18	19
SNR, dBW	-40	-30	-20	-10	-50	-50	-40	-30	-20	-10	-50	-40	-30	-20	-20
X, voxels	100	120	140	160	80	120	140	160	80	100	120	140	160	80	100
Y, voxels	120	130	140	150	110	130	140	150	110	120	130	140	150	110	120
Z, voxels	100	100	100	100	100	100	100	100	100	100	100	100	100	100	100
R, voxels	30	40	50	60	20	40	50	160	20	30	40	50	60	20	30

artifacts affect performance of our algorithm, we create *Noise* dataset by adding gaussian noise to the neuroimages in the *Normal* dataset. To quantify robustness of our algorithm with respect to such intrinsic factors as tumors and lesions, we create *Tumor* dataset by artificially growing spherical tumors of various radii and locations in the volumes from the *Normal* dataset. Noise and simulated tumor parameters are summarized in the Table 1. Finally, the fourth dataset, *Symmetric*, of perfectly symmetric brains whose iMSP has equation $x = 128$ is created by reflecting left half of every brain in the *Normal* dataset about plane $x = 128$. Since, for volumes in the *Symmetric* dataset, unlike for the volumes in the other three, we know the *exact* locations of true iMSPs, we will use it to demonstrate that our algorithm produces unbiased estimates of $\vec{V}$.
In order to evaluate accuracy of the proposed algorithm for arbitrary orientations of the

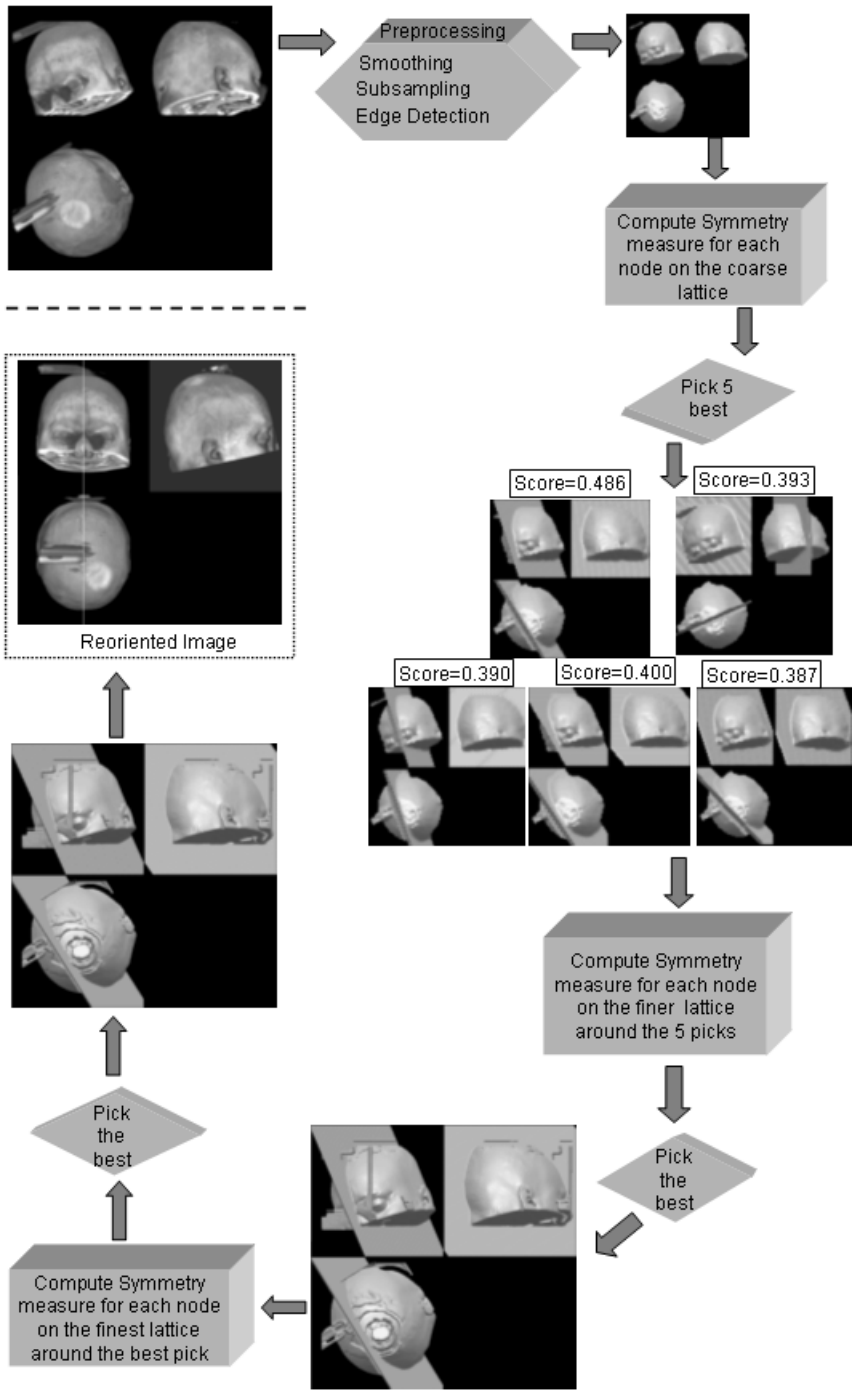

Figure 3: Illustration of the work of iMSP extraction algorithm on three orthogonal views of a 3D rendering of a MR neuroimage and a candidate MSP. First, we perform preprocessing on the input neuroimage. Then we roughly estimate five best candidate MSPs. After that we refine our estimates of the MSPs and select the best candidate. Finally, we further refine the best candidate MSP to obtain parameters of iMSP.

```
1. Preprocessing.
    Apply anisotropic diffusion to the original image.
    Find edges.
    Subsample original neuroimage.
    Find edges in the subsampled neuroimage.
    Find centroid of smallEdgeImage
    Find centroid of bigEdgeImage
2. The coarsest estimation.
    Embed lattice with mesh size of 12 degrees.
    j=0;
    for each V
      i=0;
      for(P=centroid-4V; P≤ centroid+4V; P+=V)
         Pscores[i]=computeScore(V, P, smallEdgeImage)
         i++;
      end
    Scores[j]=max(Pscores);
    j++:
    end
3. Finer Estimation.
    Find5Best_Vs (Scores);
    k=0;
    for each V
      Embed a lattice with mesh size 3 between a node
         corresponding to V and
         its neighbours
      j=0;
      for each node of the finer lattice
        i=0;
        for(P=centroid-4V; P≤ centroid+4V; P+=V)
           Pscores[i]=computeScore(V, P, smallEdgeImage)
           i++
        end
        Scores[j]=max(Pscores);
      end
    maxScores[k]=max(Scores);
    k++;
    end
    FindBestVandP(maxScores);
4. Finest Estimation
    Embed a lattice with mesh size 1.5 degrees between
a node corresponding to V and
      its neighbours
    Repeat Step 2 for this lattice and bigEdgeImage
    FindBestVandP(Scores);
5. Final Refinement.
    Embed a lattice with mesh size 0.5 degrees between
      a node corresponding to the best V found
      in step 4 and its neighbours
    Repeat step 4. for this lattice and bigEdgeImage;
return V and P found in step 5;
```

Figure 4: Pseudocode for the proposed algorithm

3D neuroimages, we apply 9 rotations R_i to every volume in each of the four datasets. We choose rotations so that each R_i is random and at the same time the set of R_i is spread out through the entire set of possible rotations. As far as midsagittal plane extraction is concerned, orientation of a volume is defined by the orientation of its iMSP, which, in turn, is defined by $\vec{V}$. Therefore, we partition the space of orientations of iMSPs into 9 sectors as illustrated by the rightmost sphere in the Figure 2 and ensure that each R_i maps $\vec{V}$ inside a different sector. In such manner we obtain 9 additional volumes for every neuroimage in each of the four datasets. This brings the total number of neuroimages in our entire testing set to $19 \times 4 \times (1 + 9) = 760$.

4.2 Sample Results

Sample results of our algorithm are presented in the Figure 5

4.3 Results of the Evaluation

For each image in our test set we know, by construction, the rotation transform R which was applied to it. Since originally midsagittal planes of the neuroimages we chose were approximately parallel to yz-plane, after we run the algorithm on an image in the test

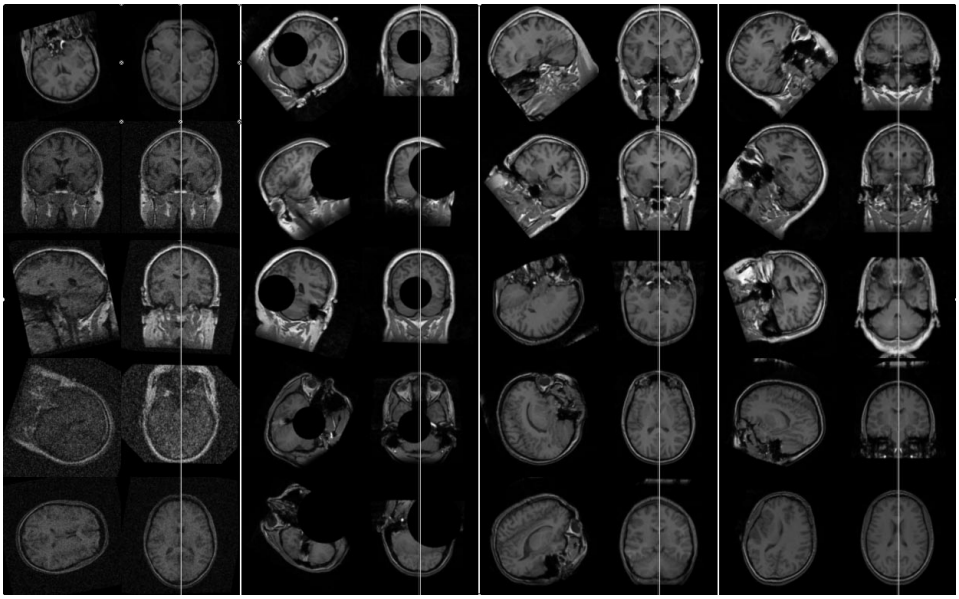

Figure 5: Leftmost column contains pairs of slices of input and reoriented brain images from *Noise* dataset. Second column from the left contains pairs of slices of input and reoriented brain images from *Tumor* dataset. Third column from the left contains pairs of slices of input and reoriented brain images from *Normal* dataset. Rightmost column contains pairs of slices of input and reoriented brain images from *Symmetry* dataset.

set, we obtain estimate E of R^{-1}. We can evaluate quality of this estimate by the angle α between the correct normal vector $\vec{V}$ and the estimated $\hat{\vec{V}}$. For each of the four datasets, for every neuroimage j and orientation i

$$\alpha_{ij} = cos^{-1} \frac{\left(E_{ij}R_{ij}[\ 1 \quad 0 \quad 0\ ]^T\right) \bullet [\ 1 \quad 0 \quad 0\ ]^T}{\left|E_{ij}R_{ij}[\ 1 \quad 0 \quad 0\ ]^T\right|} \tag{5}$$

Since in the neuroimages from *Normal, Tumor* and *Noise* datasets iMSP is only approximately parallel to yz-plane, our results for these images may be biased even if the algorithm works perfectly. To correct for this, for these three datasets, we substitute vector $\left[\ 1 \quad 0 \quad 0\ \right]^T$ in the equation (5) above by $0.1\sum_{i=1}^{10} E_{ij}R_{ij}\left[\ 1 \quad 0 \quad 0\ \right]^T$. We provide full tables of angle errors α for *Symmetric*, *Normal*, *Tumor*, *Noise* datasets in the Tables 2, 3, 4 and 5 respectively. Plots presented in Figures 6, 7 and 8. Our algorithm has mean error of 0.916 degrees when applied to *Normal* dataset, and that of 0.242 degrees when applied to *Symmetric* dataset. Our algorithm's accuracy does not suffer from noise or simulated tumors as long as signal to noise ratio is greater than -50dBW.

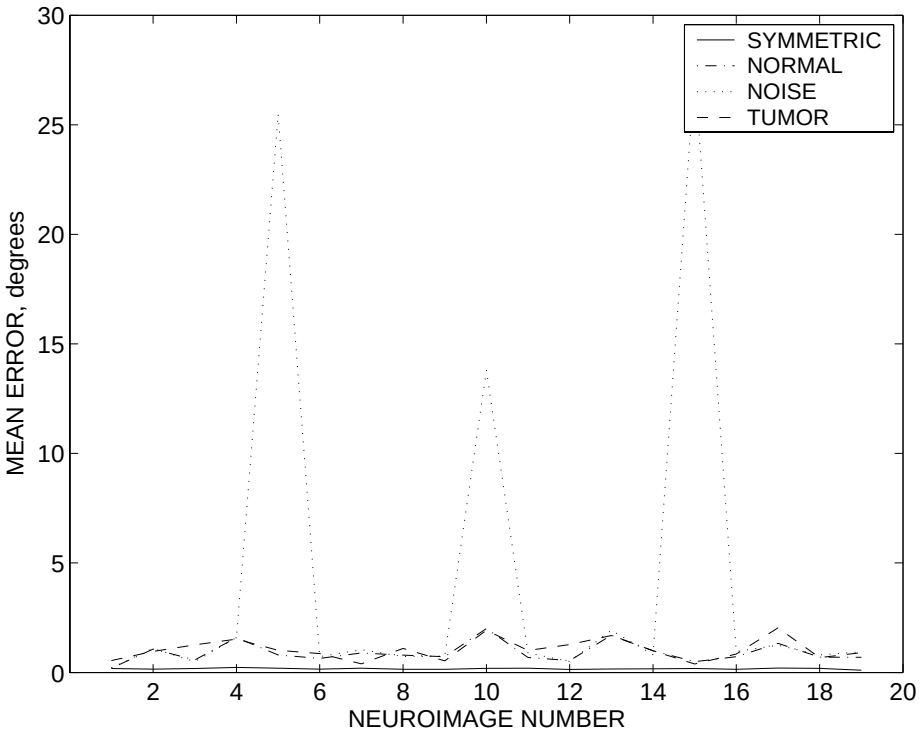

Figure 6: The graph shows breaking points of our algorithm. The algorithm failed to find iMSP for some orientations of neuroimages number 5, 10 and 15 from the *Noise* dataset. As shown in the Table 1 neuroimages 5, 10 and 15 have the strongest noise added to them. This means that in terms of noise, breaking points of the algorithm are SNR=-50dBW.

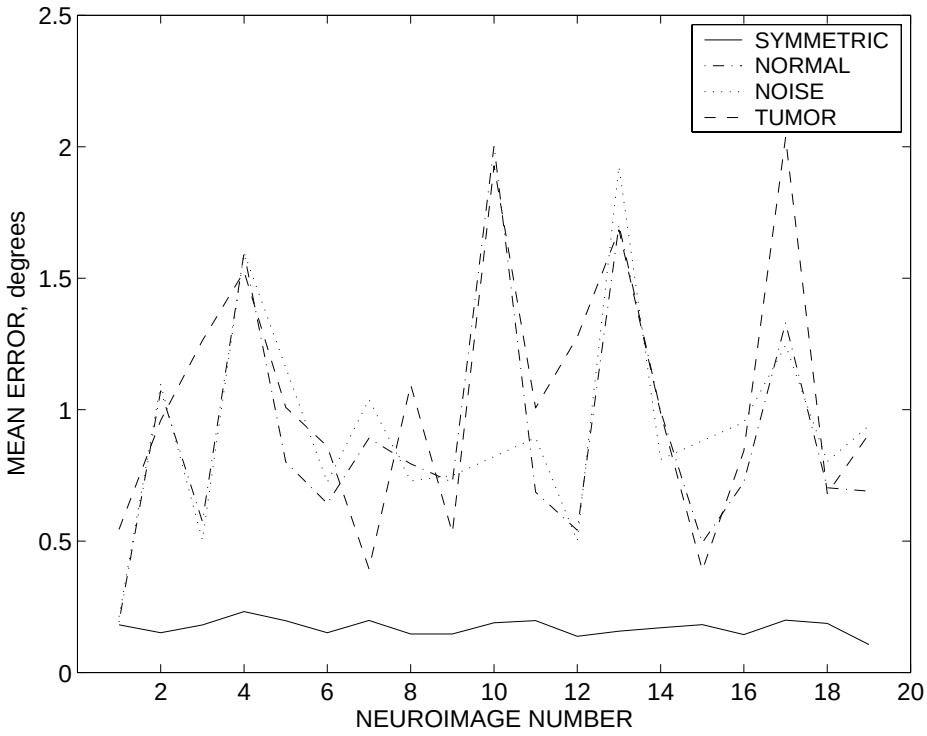

Figure 7: The graph demonstrates that below breaking points the accuracy of our algorithm does not suffer from noise or simulated tumors.

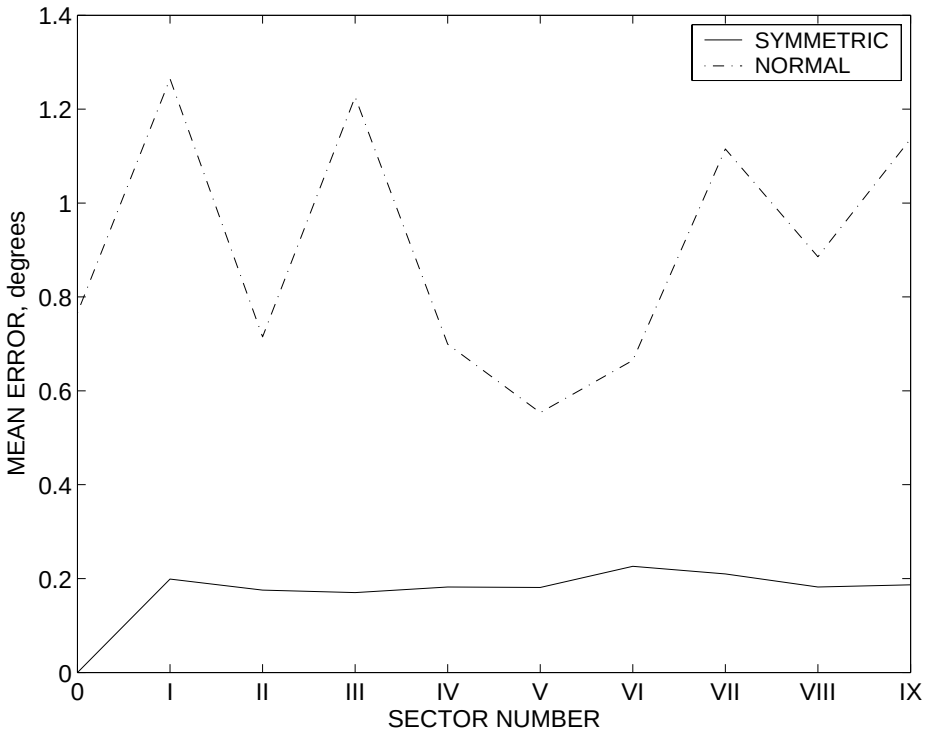

Figure 8: The leftmost graph shows errors of our algorithm for all orientations of the neuroimages in *Normal* and *Symmetric* datasets. It demonstrates that the accuracy of our algorithm does not depend on the orientation of the input brain image.

Table 2: Errors of iMSP extraction algorithm when applied to *Symmetry* dataset. For each sector(see figure 1) and neuroimage, the table contains angle, in degrees, between true and estimated orientations of the vector normal to iMSP plane. Second column corresponds to an unrotaded image, second column - to an image which is rotated so that vetor normal to its iMSP is inside sector I, and so on. Rows correspond to different neuroimages in the *Symmetry* dataset

	0	I	II	III	IV	V	VI	VII	VIII	IX	Row Mean	Row Std
1	0.000	0.311	0.128	0.194	0.076	0.245	0.270	0.138	0.199	0.256	0.182	0.096
2	0.000	0.288	0.104	0.102	0.219	0.172	0.180	0.156	0.233	0.056	0.151	0.087
3	0.000	0.193	0.074	0.280	0.217	0.302	0.239	0.227	0.123	0.150	0.181	0.094
4	0.000	0.312	0.186	0.143	0.149	0.282	0.274	0.464	0.282	0.226	0.232	0.124
5	0.000	0.111	0.218	0.201	0.267	0.037	0.356	0.376	0.179	0.224	0.197	0.123
6	0.000	0.123	0.119	0.328	0.058	0.108	0.223	0.214	0.081	0.258	0.151	0.101
7	0.000	0.252	0.167	0.254	0.119	0.199	0.275	0.269	0.232	0.215	0.198	0.085
8	0.000	0.288	0.156	0.066	0.105	0.128	0.243	0.157	0.141	0.181	0.146	0.082
9	0.000	0.210	0.277	0.105	0.224	0.096	0.110	0.113	0.137	0.193	0.146	0.080
10	0.000	0.142	0.267	0.230	0.175	0.295	0.262	0.207	0.208	0.107	0.189	0.088
11	0.000	0.271	0.301	0.104	0.241	0.143	0.254	0.265	0.229	0.167	0.198	0.093
12	0.000	0.165	0.066	0.141	0.083	0.189	0.168	0.190	0.301	0.075	0.138	0.085
13	0.000	0.050	0.322	0.196	0.200	0.119	0.210	0.084	0.306	0.085	0.157	0.107
14	0.000	0.182	0.253	0.120	0.259	0.197	0.166	0.174	0.070	0.282	0.170	0.088
15	0.000	0.227	0.113	0.218	0.346	0.161	0.256	0.082	0.172	0.246	0.182	0.099
16	0.000	0.195	0.110	0.044	0.171	0.174	0.104	0.265	0.118	0.261	0.144	0.086
17	0.000	0.293	0.180	0.229	0.245	0.240	0.300	0.184	0.075	0.248	0.199	0.095
18	0.000	0.113	0.207	0.198	0.225	0.247	0.256	0.283	0.188	0.148	0.187	0.083
19	0.000	0.059	0.088	0.076	0.081	0.105	0.155	0.139	0.190	0.169	0.106	0.057
Column Mean	0.000	0.199	0.175	0.170	0.182	0.181	0.226	0.210	0.182	0.187	Total Mean	Total Std
Column Std	0.000	0.084	0.080	0.078	0.079	0.074	0.065	0.096	0.072	0.069	0.171	0.093

Table 3: Errors of iMSP extraction algorithm when applied to *Normal* dataset. For each sector(see figure 1) and neuroimage, the table contains angle, in degrees, between true and estimated orientations of the vector normal to iMSP plane. Second column corresponds to an unrotaded image, second column - to an image which is rotated so that vetor normal to its iMSP is inside sector I, and so on. Rows correspond to different neuroimages in the *Normal* dataset

	0	I	II	III	IV	V	VI	VII	VIII	IX	Row Mean	Row Std
1	0.100	0.283	0.064	0.175	0.072	0.178	0.337	0.237	0.252	0.222	0.192	0.092
2	0.702	0.675	1.003	2.815	0.490	0.508	0.431	0.944	0.816	2.329	1.071	0.821
3	0.654	0.453	0.857	0.675	0.474	0.305	0.621	0.695	0.463	0.544	0.574	0.158
4	0.788	4.775	1.372	2.159	0.926	0.897	0.497	0.965	1.750	1.836	1.596	1.236
5	1.446	0.675	0.208	0.966	0.833	0.097	0.887	0.603	1.601	0.695	0.801	0.472
6	1.308	0.693	0.828	1.030	0.359	0.410	0.557	0.082	0.615	0.549	0.643	0.349
7	0.687	0.964	1.458	0.660	0.758	0.640	1.113	0.338	1.011	1.287	0.892	0.338
8	0.050	0.784	0.751	1.364	0.462	0.775	0.253	2.325	0.473	0.702	0.794	0.645
9	0.234	0.869	0.679	1.741	0.711	0.300	0.183	0.741	0.631	1.144	0.723	0.466
10	1.382	3.783	0.364	1.844	1.703	1.921	1.567	2.603	1.666	3.197	2.003	0.969
11	0.135	1.840	0.575	1.246	0.363	0.236	0.469	0.730	0.506	0.759	0.686	0.512
12	0.991	0.705	0.478	0.438	1.204	0.352	0.192	0.409	0.247	0.397	0.541	0.328
13	1.523	2.046	1.601	1.509	2.337	0.922	1.274	2.496	1.537	1.774	1.702	0.478
14	2.129	1.223	0.295	1.163	0.531	0.457	0.671	1.370	1.156	0.946	0.994	0.541
15	0.089	1.028	0.389	0.746	0.352	0.454	0.345	0.599	0.260	0.677	0.494	0.272
16	0.222	0.274	0.441	0.936	0.501	0.302	1.290	0.501	1.041	1.734	0.724	0.505
17	0.726	1.093	1.007	2.157	0.263	0.885	0.857	3.529	0.910	1.869	1.330	0.947
18	0.449	0.701	0.727	1.250	0.512	0.174	0.337	1.365	0.903	0.607	0.702	0.380
19	0.945	1.165	0.482	0.425	0.436	0.705	0.755	0.659	0.991	0.335	0.690	0.277
Column Mean	0.766	1.265	0.715	1.226	0.699	0.554	0.665	1.115	0.886	1.137	Total Mean	Total Std
Column Std	0.585	1.165	0.426	0.684	0.541	0.420	0.405	0.946	0.486	0.791	0.903	0.716

Table 4: Errors of iMSP extraction algorithm when applied to *Tumor* dataset. For each sector(see figure 1) and neuroimage, the table contains angle, in degrees, between true and estimated orientations of the vector normal to iMSP plane. Second column corresponds to an unrotaded image, second column - to an image which is rotated so that vetor normal to its iMSP is inside sector I, and so on. Rows correspond to different neuroimages in the *Tumor* dataset

	0	I	II	III	IV	V	VI	VII	VIII	IX	Row Mean	Row Std
1	0.255	2.449	0.235	0.442	0.215	0.458	0.402	0.581	0.245	0.159	0.544	0.683
2	1.210	0.965	1.174	2.719	0.471	0.262	0.657	0.839	0.154	1.140	0.959	0.724
3	0.987	1.121	1.149	1.665	1.218	0.977	1.546	1.287	1.189	1.484	1.262	0.233
4	0.659	4.696	1.444	1.958	0.795	1.050	0.402	0.930	1.828	1.486	1.525	1.223
5	1.479	0.674	0.567	0.437	1.478	0.799	1.587	0.629	1.450	0.984	1.008	0.446
6	1.498	0.687	0.323	1.110	0.795	0.366	0.972	0.489	1.481	0.881	0.860	0.418
7	0.213	0.427	1.014	0.595	0.323	0.304	0.085	0.298	0.478	0.207	0.394	0.262
8	0.201	1.014	0.615	1.525	1.187	0.902	1.714	2.623	0.581	0.590	1.095	0.707
9	0.349	0.410	0.860	1.085	0.245	0.127	0.372	0.622	0.427	0.809	0.531	0.304
10	0.814	4.387	1.032	2.008	1.969	0.864	1.269	2.147	1.985	2.800	1.928	1.079
11	0.545	2.106	0.769	0.943	1.820	0.626	0.696	1.009	0.869	0.682	1.006	0.528
12	1.511	1.339	3.037	1.797	0.965	1.313	0.269	1.282	0.627	0.622	1.276	0.774
13	1.110	1.710	3.470	1.586	0.797	1.509	1.204	2.994	1.101	1.359	1.684	0.865
14	0.712	1.151	0.468	2.053	0.745	0.580	0.827	1.532	1.033	0.772	0.987	0.483
15	0.128	0.756	0.225	0.218	0.423	0.138	0.378	0.642	0.294	0.686	0.389	0.232
16	0.899	0.483	0.887	0.771	0.751	0.265	2.166	0.765	0.834	0.612	0.843	0.505
17	1.065	2.672	1.931	3.486	0.328	3.467	1.249	1.392	1.025	3.733	2.035	1.218
18	0.482	0.754	0.775	1.204	0.459	0.223	0.350	1.481	0.423	0.653	0.680	0.395
19	0.605	1.600	0.330	1.612	0.241	0.304	0.483	1.289	1.664	0.944	0.907	0.588
Column Mean	0.775	1.547	1.069	1.432	0.801	0.765	0.875	1.202	0.931	1.084	Total Mean	Total Std
Column Std	0.454	1.244	0.886	0.824	0.527	0.769	0.586	0.726	0.556	0.863	1.048	0.801

Table 5: Errors of iMSP extraction algorithm when applied to *Noise* dataset. For each sector(see figure 1) and neuroimage, the table contains angle, in degrees, between true and estimated orientations of the vector normal to iMSP plane. Second column corresponds to an unrotaded image, second column - to an image which is rotated so that vetor normal to its iMSP is inside sector I, and so on. Rows correspond to different neuroimages in the *Noise* dataset

	0	I	II	III	IV	V	VI	VII	VIII	IX	Row Mean	Row Std
1	0.033	0.243	0.109	0.374	0.069	0.224	0.371	0.166	0.283	0.251	0.212	0.118
2	1.088	0.752	1.089	3.266	0.418	0.281	0.559	0.861	0.497	2.141	1.095	0.928
3	0.629	0.468	0.886	0.642	0.278	0.265	0.638	0.664	0.484	0.085	0.504	0.238
4	0.788	4.775	1.372	2.159	0.926	0.897	0.497	0.965	1.750	1.836	1.596	1.236
5	79.522	12.601	12.277	78.977	12.938	12.524	12.405	12.435	8.928	12.292	25.490	28.357
6	1.203	0.482	0.494	1.699	0.465	0.450	1.201	0.898	0.082	0.258	0.723	0.508
7	0.709	1.070	0.901	0.605	1.185	0.707	1.004	1.434	1.344	1.422	1.038	0.307
8	0.561	0.443	0.954	0.938	0.452	0.468	0.538	1.501	0.567	0.867	0.729	0.338
9	0.274	0.837	1.442	1.495	0.469	0.363	0.332	0.501	0.389	1.385	0.749	0.502
10	5.525	6.537	5.393	5.774	7.054	79.702	5.479	5.270	8.254	8.889	13.788	23.194
11	0.967	1.292	0.892	0.703	2.444	0.152	0.736	0.684	0.739	0.322	0.893	0.630
12	0.512	0.631	0.514	0.460	0.572	0.683	0.216	0.790	0.223	0.410	0.501	0.185
13	1.317	2.336	3.274	1.338	2.271	1.460	1.468	3.440	1.418	0.924	1.925	0.869
14	1.065	0.924	0.374	1.336	0.517	0.165	0.635	1.723	0.835	0.532	0.811	0.470
15	82.207	7.963	12.975	8.275	6.881	46.392	8.004	8.215	85.315	7.681	27.391	32.015
16	0.909	0.861	0.325	1.271	1.136	0.905	1.244	1.199	1.026	0.641	0.952	0.296
17	0.723	0.922	1.460	2.200	0.707	0.314	0.262	2.579	1.437	1.844	1.245	0.791
18	0.613	0.795	0.904	1.255	0.432	0.386	0.805	1.398	0.810	0.626	0.802	0.325
19	1.137	1.090	1.075	1.965	0.727	0.533	0.635	0.542	1.205	0.482	0.939	0.456
Column Mean	9.462	2.370	2.458	6.039	2.102	7.730	1.949	2.382	6.083	2.257	Total Mean	Total Std
Column Std	25.191	3.300	3.781	17.771	3.316	20.456	3.211	3.125	19.347	3.423	4.283	13.399

5. iMSP and Registration.

Process of neuroimage registration can benefit greatly from iMSP extraction. First, reorienting two neuroimages that we would like to register according to their iMSPs brings them closer together and helps registration avoid many local extrema. Second, by requiring that iMSPs of two registered neuroimages coincide, we reduce the number of parameters a registration procedure has to optimize. In the case of rigid registration, for example, 6 continuous parameters can be reduced to 4: three continuous representing rotation parallel to iMSP and 2 translations, and one binary representing flip. To evaluate advantages for registration provided by our iMSP extraction algorithm, we conducted experiments using 190 neuroimages from *Normal* dataset. We used rigid registration algorithm available in Insight Toolkit [8] with mean intensity square difference as a similarity measure and MIRIT algorithm [13] for affine registration using mutual information [20]. Our experiments have shown that reducing number of degrees of freedom using constraints imposed by iMSP makes registration more than twice as fast compared to mere alignment of iMSPs of two images without sacrificing quality of registration. Our other findings in terms of reliability and accuracy of registration

which employs midsagittal plane extraction are presented in Figures 9, 10 and 11.

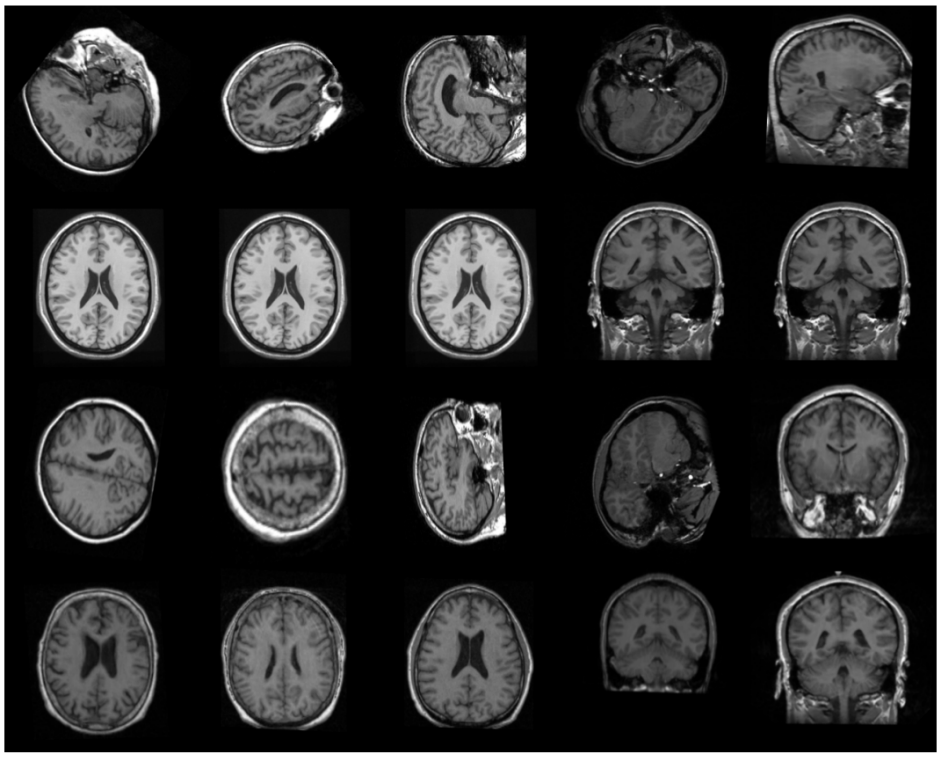

Figure 9: Advantage of using iMSP for registration. First row contains the slices of an input neuroimage we are about to register. Second row contains a slice of the target neuroimage to which we register the input brain image. Third row contains the result of registration without reorienting input brain image according to iMSP. Fourth row contains results of registration after reorientation had been applied.

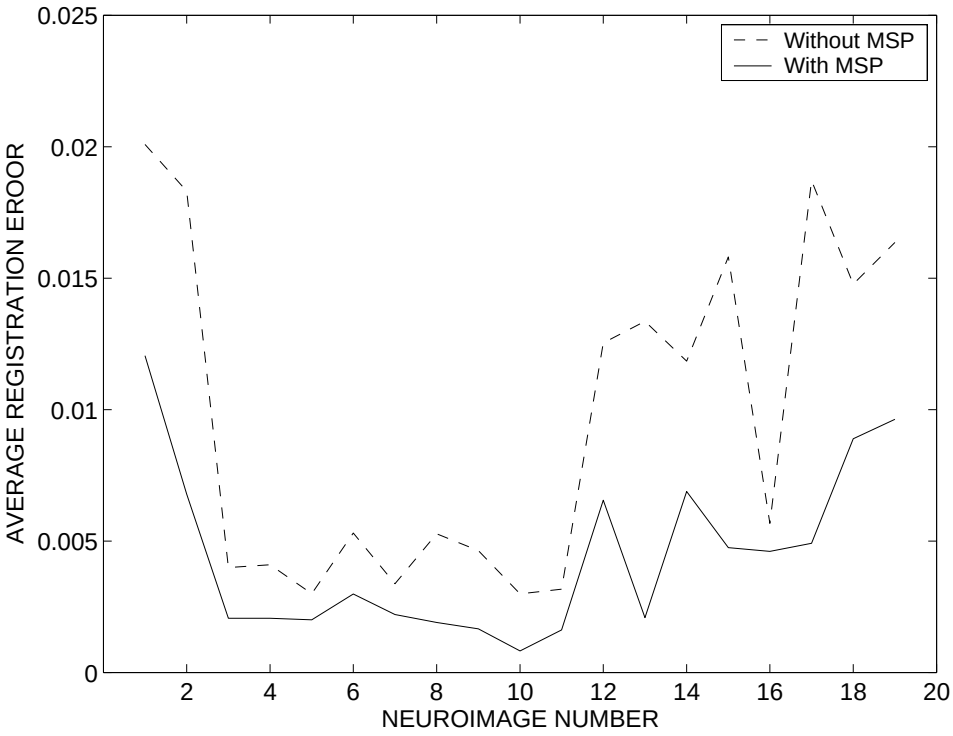

Figure 10: The graph shows that accuracy of registration is improved for every brain image when iMSP extraction algorithm is applied before the registration.

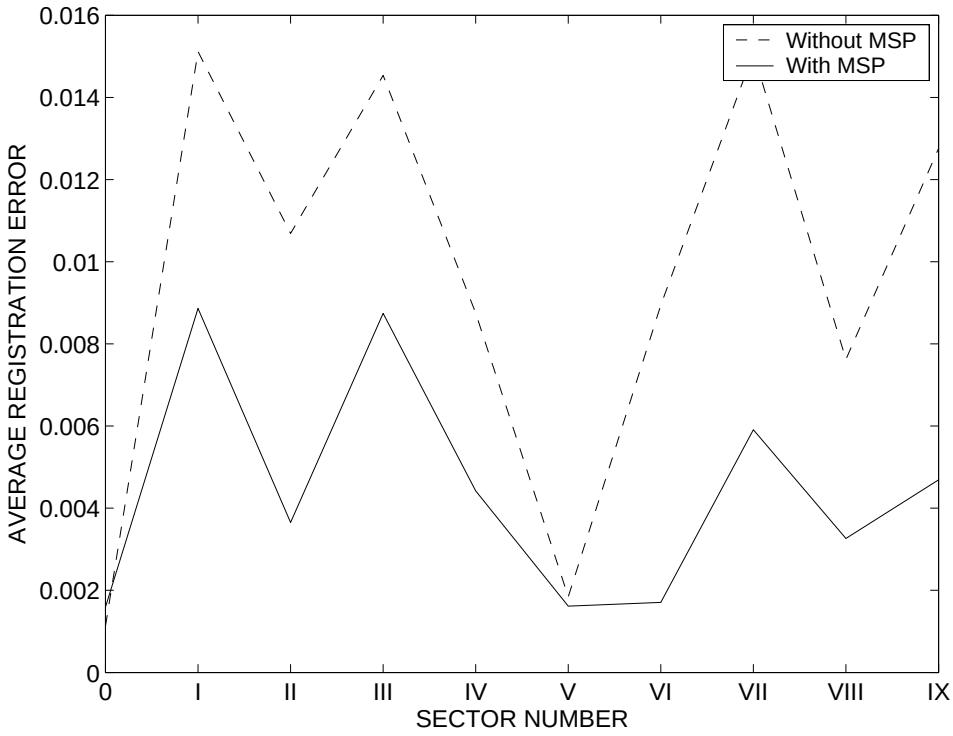

Figure 11: The graph shows that accuracy of registration is improved for every orientation when iMSP extraction algorithm is applied before the registration.

6. Summary and Conclusions

We have presented a robust truly three dimensional algorithm for ideal midsagittal plane extraction. We have shown that, unlike other existing algorithms, our algorithm has no limitations on the initial orientation of the input neuroimage while achieving accuracy comparable to that of existing algorithms. In addition, we have demonstrated and quantitatively evaluated the improvements in registration accuracy, speed and reliability of neuroimage registration that are made possible by our ideal midsagittal plane extraction algorithm.

7. Acknowledgments

The algorithm was implemented using Insight Toolkit that allowed us to write efficient code in short period of time, for which we are grateful. Using the toolkit we can completely estimate midsagittal plane for a 256 by 256 by 256 neuroimage in less than

3 minutes on a Pentium 4 2.6Ghz processor running Windows XP. We will contribute our algorithm to be a part of Insight Toolkit in the nearest future.

References

[1] Ardekani, B., Kershaw, J., Braun, M., and Kanno, I. *Automatic detection of the mid-sagittal plane in3-d brain images.* IEEE Transactions on Medical Imaging 16(6): 947952, 1997

[2] Brummer, M. *Hough transform detection of the longitudal fissure in tomographic head images.* IEEE Transactions on Medical Imaging 10(1): 7481, 1991

[3] Canny, J. *A Computational approach to edge detection.* IEEE Pattern Analysis and Machine Intelligence, 8(6):679-698, 1986.

[4] Crow, T. *Schizophrenia as an anomaly of cerebral asymmetry.* In K. Maurer, editor, *Imaging of the brain in psuchiatry and related fields.* Springer-Verlag, 1993.

[5] Geschwind, N. and Levitsky, W. *Human brain: left-right asymmetries in temporal speech region.* Science, 161:186-187, 1968.

[6] Guillemaud, R., Marais, P., Zisserman, A., McDonald, T., and Crow, B. *A 3-dimensional midsagittal plane for brain asymmetry measurement.* Schizophrenia Research 18(2-3):183184, 1995

[7] Junck, L., Moen, J., Hutchins, G., Brown, M., and Kuhl, D. *Correlation methods for centering, rotation, and alignment of functional brain images.* Journal of Nulear Medicine, 31(7): 12201226, 1990

[8] Ibanez, L., Schroeder, W., Ng, L., Cates, J. *ITK Software Guide* Kitware, Inc., 2003.

[9] Liu, Y., Collins, R., and Rothfus, W., *Robust Midsagittal Plane Extraction from Normal and Pathological 3-D Neuroradiology Images,* IEEE Transactions on Medical Imaging, 2001.

[10] Liu, Y. and Dellaert, F. *A classification-based similarity metric for 3D image retreival.* In Proceedings of Computer Vision and Pattern Recognition Conference, pages 800:805, June 1998.

[11] Liu, Y., Dellaert, F., and Rothfus, E *Classification-driven semantic based medical image indexing and retreival.* Techbical Report CMU-RI-TR-98-25, The Robotics Institute, Carnegie Mellon University, Pittsburgh, PA, 1998.

[12] Liu, Y., Rothfus, E., and Kanade, T. *Content based 3d neuroradiologic image retreival: Preliminary results.* IEEE Workshop on Content-Based Access of Image and Video Libraries, in conjunction with International Conference of Computer Vision, pages 91, 100, January 1998.

[13] Maes, F, Collignon, A, Vandermeulen, D., Marchal, G., P. Suetens *Multimodality image registration by maximization of mutual information* IEEE transactions on Medical Imaging 16(2):187-198, 1997.

[14] Matsuda, T., Yamamoto, K., and Yamada, H. *Detection of partial symmetry using correlation with rotated-reflected images.* Pattern Recognition, 26(8):1245, 1253, 1993.

[15] Minoshima, S., Berger, K., Lee, K., and Mintum, M. *An automated method for rotational correction and centering of three-dimensional functional brain images.* Journal of Nuclear Medicine, 33(8): 15791585, 1992

[16] Perona, P., and Malik, J. *Scale-space and edge detection using anisotropic diffusion.* IEEE Trans. on Pattern Analysis and Machine Intelligence, Vol. 12, No. 7, pp. 629-639, 1990.

[17] Prima, S., Oursein, S., Ayache, N. *Computation of the mid-sagittal plane in 3-D brain images* IEEE Transactions on Medical Imaging 21(2): 122138, 2002

[18] Talairach, J. and Tournoux, P. *Co-Planar Steriotaxic Atlas of the Human Brain* Thieme Medical Publishers, 1988.

[19] Thirion, J., Prima S., and Subsol, G. *Statistical analysis of normal and abnormal dissymetry in volumetric medical images.* In Proceedings of Workshop on Biomedical Image Analysis, pages 74-83. IEEE Computer Society, 1998.

[20] Wells, W., Viola, P., Atsumi, H., Nakajima, S. and Kikinis, R. *Multi-modal volume registration by maximization of mutual information.* Medical Image Analysis, 1(1):35-51, March 1996.